NASA Technical Memorandum 81740

The Fracture Morphology of Nickel-Base Superalloys Tested in Fatigue and Creep-Fatigue at 650° C

John Gayda and Robert V. Miner
Lewis Research Center
Cleveland, Ohio

April 1981

NASA

THE FRACTURE MORPHOLOGY OF NICKEL-BASE SUPEPALLOYS TESTED IN FATIGUE AND CREEP-FATIGUE AT 650° C

by John Gayda and Robert V. Miner

National Aeronautics and Space Administration
Lewis Research Center
Cleveland, Ohio 44135

SUMMARY

The fracture surfaces of compact tension specimens from seven nickel-base superalloys fatigue tested at 650° C were studied by scanning electron microscopy and optical metallography to determine the nature and morphology of the crack surface in the region of stable growth. Crack propagation testing was performed as part of an earlier study at 650° C in air using a 0.33 Hz fatigue cycle and a creep-fatigue cycle incorporating a 900 second dwell at maximum load. The alloys studied included HIP Astroloy, Waspaloy, HIP plus forged Astroloy, MERL 76, IN 100, René 95, and NASA IIB-7. Each alloy is gamma prime strengthened, but composition, microstructure, and strength levels vary from alloy to alloy.

In fatigue, alloys with a grain size greater than 20 μm, HIP Astroloy, Waspaloy, and MERL 76, exhibited transgranular fracture. MERL 76 also displayed numerous fracture sites which were associated with boundaries of prior powder particles. This behavior was especially noticeable at higher stress levels. The two high strength, fine grain alloys, IN 100 and NASA IIB-7, exhibited intergranular fracture. Rene 95 and HIP plus forged Astroloy, which possess a necklace structure, displayed a mixed failure mode that was transgranular in the coarse grains and intergranular in the fine grains. Fatigue crack growth rates were lowest for the low strength, coarse grain alloys which failed in a transgranular fashion.

Under creep-fatigue conditions, fracture was found to be predominantly intergranular in all seven alloys; however, two of the alloys displayed additional features. Waspaloy also fractured at twin boundaries on occasion, while numerous prior particle fracture sites were again observed in MERL 76. As in fatigue, the crack growth rate of the low strengtn, coarse grain alloys were lowest, but tne crack growth rate of all alloys increased significantly under creep-fatigue conditions.

E-793

INTRODUCTION

Fatigue is known to be a limiting factor affecting the useful life of aircraft turbine engine disks. Both initiation and propagation of fatigue cracks are important aspects of the overall problems. Furthermore, in the rim of high performance turbine disks where temperatures can approach 650° C, time dependent effects arising from creep-fatigue-environment interactions[1-2] may further complicate the problem. NASA has recently sponsored studies[3-6] to examine the fatigue and creep-fatigue behavior of seven turbine disk alloys, HIP Astroloy, Waspaloy, HIP-plus-forged (H+F) Astroloy, MERL 76, IN 100, René 95, and NASA IIB-7, all of which are gamma-prime (γ') strengthened, nickel-base superalloys. These alloys include both a cast and wrought alloy, Waspaloy, as well as several of the latest generation powder metallurgy alloys representing a wide range of strength levels.

Crack propagation behavior was studied with compact tension specimens at a temperature of 650° C, which may be representative of critical rim locations in high performance turbine disks. To study time dependent effects, a fast fatigue cycle, 0.33 Hz, and a creep-fatigue cycle, incorporating a 900 second tensile dwell at maximum load, were evaluated.

The results of these studies have shown the higher strength alloys, IN 100, René 95, and NASA IIB-7, possess longer total fatigue lives below one percent strain range, compared with the low strength alloys, HIP Astroloy and Waspaloy, due to an increased resistance to crack initiation. Crack propagation rates are, however, much higher for the high strength alloys particularly in creep-fatigue.

In the present investigation, crack propagation test specimens from the previous studies[4-6] were examined in detail in an attempt to correlate failure mode, crack growth rates, and metallurgical structure. The crack growth results of the earlier studies[4-6] are summarized in this paper and are correlated with local fracture morphology for all seven alloys. In addition, the fracture morphology is related to cycle type and the stress intensity range.

MATERIALS AND PROCEDURES

Materials

All materials used in this study were obtained from turbine disk preforms with the exception of NASA IIB-7, which was procured as plate. The microstructures of the seven nickel-base superalloys studied herein are presented in figure 1. The chemical composition, mechanical properties, and heat treatments can be found in tables I and II. These alloys are all γ' strengthened, but their γ' content, morphology, and distribution vary widely, as shown in table III. A more detailed description of each alloy is presented below.

HIP Astroloy was produced by hot isostatically pressing low carbon Astroloy powder for 3 hours at 1190° C and 104 MPa. The alloy is not subsequently forged and the resulting structure, after heat treatment, contains 44 percent γ' which was determined by electrolytic extraction procedures.[7] In this alloy, about half of the γ' is present as cube shaped particles 0.1 to 1.0 μm in size. The remainder is uniformly distributed throughout as finer particles about 0.03 μm. The grain size is nearly uniform in this material at 50 to 70 μm.

Waspaloy, produced by forging a cast billet, contains approximately 20 percent γ', which occurs as a uniform distribution of spherical particles about 0.03 μm in diameter and an occassional particle about 0.3 μm in diameter. The grain size is predominantly 40 to 150 μm. Grain boundary carbides of the $M_{23}C_6$ and MC type[7] clearly delineate the grains, as seen in figure 1.

H+F Astroloy was forged from a HIP processed powder billet. A necklace structure is produced by the forging operation, in which large grains, 50 to 100 μm, are surrounded by fine, recrystallized grains, 15 μm and less. The alloy contains 42 percent γ', which occurs as large blocky particles 0.5 to 3.0 μm concentrated in the fine, recrystallized grains and smaller, more uniform particles about 1.0 μm in the larger grains. In addition, fine γ' particles 0.3 and 0.04 μm are uniformly distributed throughout.

MERL 76, another powder metallurgy alloy, was hot isostatically pressed at 1182° C for 3 hours at 103 MPa, but was not forged. After heat treat-

ment, the alloy contains 60 percent γ' of which about half is present as large blocky particles 0.5 to 5.0 μm in size. The remaining γ' is composed of smaller particles 0.2 and 0.03 μm. In this alloy, the grain size is nearly uniform at 15 to 20 μm. A dendritic solidification structure is apparent in many grains.

IN 100 was produced by the Gatorizing™ process, in which powder is hot compacted, extruded, and then isothermally forged at a low strain rate where material behavior is superplastic. After heat treatment, the alloy has a γ' content of 62 percent, of which about half is present as large blocky particles 0.5 to 5.0 μm in size, while the balance is uniformly distributed as finer particles 0.05 to 0.15 μm. The grain size is quite uniform at 4 to 6 μm.

René 95 was forged from a HIP processed powder billet. It contains 50 percent γ' after heat treatment. This alloy has a necklace structure in which large grains, 50 to 70 μm, are surrounded by fine, recrystallized grains, 15 μm and less. The γ' is present as large blocky particles 0.5 to 4 μm concentrated in the necklace grains and smaller particles 0.5 to 1 μm, which are found in the larger grains. Fine γ' particles 0.03 to 0.06 μm are also uniformly distributed throughout.

The last alloy, NASA IIB-7, was made by hot isostatically pressing argon-atomized powder for two hours at 1215° C and 100 MPa, followed by an intermediate heat treatment, and then cross-rolling at 1065° C to a 55 percent reduction in thickness. This alloy, after a final heat treatment, contains 59 percent γ'. About half of the γ' is composed of large blocky particles 0.5 to 5.0 μm in size, while the balance is uniformly distributed as smaller particles 0.03 to 0.06 μm. The grain size is 4 to 6 μm.

Crack Growth Testing

Crack propagation data were obtained on the seven superalloys using compact tension specimens[4-6] illustrated in figure 2. Testing was done in air at 650° C using a servohydraulic, closed-loop, load-controlled test machine operated in tension at a frequency of 0.33 Hz and a load ratio (minimum load/maximum load) of 0.05. A simple triangular waveform was used for fatigue loading while a 900 second dwell at maximum load was added to the simple fatigue waveform for creep-fatigue loading. All specimens were precracked at room temperature in accordance with ASTM E-399. Both fatigue and creep-fatigue testing was continued until total specimen failure occurred. During the test, crack growth was checked at regular intervals with a traveling microscope, after cooling the specimen. From this information, discrete values of $\Delta a/\Delta N$ (crack length/cycle) versus ΔK (stress intensity range) were plotted, through which a smooth curve was constructed based on the hyperbolic sine model.[8] The basic equation describing this model is presented below:

$$\log(da/dn) = C_1 \sinh(C_2(\log(\Delta K)) + C_3) + C_4$$

The coefficients, C_1 through C_4, are determined by regression analysis of the raw data.

Fractography

The fracture surfaces of the compact tension specimens were examined with a scanning electron microscope. All fractographs were taken along the

centerline of the specimen, starting in the precrack region and terminating in the fast fracture region. Further, the location of each fractograph was accurately recorded with respect to the precrack interface so the crack length and stress intensity range could be computed and correlated with local fracture morphology.

Optical micrographs were also used to characterize fracture morphology. Sections perpendicular to the direction of crack propagation were cut from the compact tension specimens, mounted, polished, and some were etched in a 10 percent solution of H_2O_2 (30 percent) in concentrated HCl acid. These specimens were examined in the etched and unetched condition with a metallurgical microscope and the scanning electron microscope. The position of each section with respect to the precrack interface was noted so the crack length and stress intensity range could be calculated and correlated with local fracture morphology.

RESULTS AND DISCUSSION

Crack Growth Rates

Results of the crack propagation tests,[3-5] in which growth rates are plotted as a function of the stress intensity range, are reproduced in figure 3 for fatigue tests and in figure 4 for the creep-fatigue tests. Each of these curves are an average of at least three trials although not all of the individual tests cover the range shown.

Those alloys with lower yield strengths at 650° C generally exhibit lower crack propagation rates in fatigue, as seen in table II. However, an exact ranking of crack growth rates with strength did not exist. The most notable exception to the ranking of the alloys was NASA IIB-7, the strongest alloy, and Rene 95. Over the range of the data, Rene 95 displayed the highest crack growth rate of any alloy tested. The ranking for HIP Astroloy and Waspaloy was also inverted relative to yield strength above 25 MPa $\sqrt{m}$. The crack propagation data shown in figure 3 tends to converge at low values of the stress intensity range, suggesting these alloys have a similar threshold stress intensity under fatigue loading.

In all instances, the crack growth rates for the creep-fatigue conditions increased at least one order of magnitude over the fatigue tests, with the stronger alloys exhibiting a much more pronounced increase. In comparison to the fatigue crack propagation data, the crack growth rates for the creep-fatigue test exhibit a greater spread between alloys. Once again, the lower strength alloys tend to have lower crack propagation rates; however, an exact ranking between crack propagation and strength is lacking. The order of NASA IIB-7 and René 95 is again inverted relative to yield strength with Rene 95 having the highest crack growth rate over the range of the data.

Fracture Morphology

At low magnification, the fracture surface morphology of all specimens can be divided into three regions which correspond to room temperature precracking, stable crack growth at temperature, and final fast fracture. These three regions are clearly seen in figure 5 for the fatigue and creep-fatigue test cycle. In most cases, the stable crack growth region of the fatigue specimens was flat. However, on the creep-fatigue specimens parallel ridges originating at the precrack interface ran down the length of the fracture surface. The severity and depth of these ridges increased with increasing crack length as seen in figure 5.

Although the fracture morphology of the precrack region was different from that in the fast fracture region, these regions varied little among alloys or test cycles. Precracking at room temperature produced transgranular fracture for all alloys, while the fast fracture region exhibited a dimpled appearance characteristic of tensile failures[9] with occasional cleavage-like facets.

Fatigue. - Under fatigue conditions, the fracture mode associated with stable crack growth varied from alloy to alloy. Waspaloy and HIP Astroloy, with grain sizes greater than 40 μm, exhibited a transgranular fracture mode as seen in figure 6. These two alloys also displayed the lowest crack growth rates. The two fine grain alloys, IN 100 and NASA IIB-7, exhibited an intergranular fracture mode as seen in figure 7. Their crack growth rates were greater than those of Waspaloy or HIP Astroloy.

Alloys which possessed the necklace structure, H+F Astroloy and René 95, exhibited a mixed fracture mode when tested in fatigue at 0.33 Hz. The fine recrystallized grains failed along grain boundaries, while the larger grains showed a transgranular failure mode as seen in figure 8. H+F Astroloy was more resistant to crack propagation than the high strength, fine grain alloys, but not as resistant as the low strength, coarse grain material. René 95, as previously stated, exhibited the highest crack growth rate, but it was neither the strongest alloy nor did it possess the finest grain size. Ranking crack growth rate with grain size is somewhat ambiguous for these alloys since cracking was both transgranular in the coarse grains and intergranular in the fine, recrystallized necklace grains. Therefore, a ranking of crack growth rate with either grain size in these alloys could be misleading.

Fatigue failure in MERL 76, with a grain size of 15 to 20 μm, was basically transgranular. However, occasional fracture along prior particle boundaries (PPB) was observed as seen in figure 9. The frequency of the PPB fracture sites increased as the crack grew and stress level increased, being most severe in the fast fracture region. Fracture along the PPB's was believed to have been caused by a thin hafnium rich oxide layer found on the surface of the larger powder particles. These particles were found to be present throughout the powder blend used to fabricate the disk from which the specimens were cut.[10] Oxidized powder particles were not found in other blends of MERL 76. The crack growth rate of the specimens exhibiting PPB fracture sites was intermediate compared to the other alloys. A subsequent crack growth test run at a lower stress level, but equivalent stress intensity range, virtually eliminated the PPB fracture mode in the stable crack growth region. PPB fracture sites were still observed near and in the fast fracture zone where stress levels are highest. The crack growth rate of this specimen was dramatically decreased (fig. 10) and approached that of HIP Astroloy which also exhibited transgranular fracture. This result is believed to reflect the behavior of MERL 76 when high quality powder is used.

At lower stress intensities, under fatigue conditions, fracture detail was more closely associated with microstructural features, especially grain size. This behavior was most readily seen in H+F Astroloy (fig. 11(a)) where failure was intergranular in the fine grains and transgranular in the coarse grains. As the crack grew, two prominent changes were observed. First, the transgranular fracture surfaces developed deep secondary cracks which were approximately aligned with the main crack front. Such cracks have been observed before and are associated with slip band cracking and cleavage[11]. Second, the fine grain areas, which fractured along grain boundaries at lower stress intensity ranges, begin to show some regions

which appear to have failed in a transgranular manner as seen in figure 11(b). These results are consistent with the observations of others at high stress intensity ranges,[12] and have been attributed to the development of a large plastic zone ahead of the crack tip.[11]

In summary, fatigue crack propagation was transgranular when the grain size exceeded 20 μm. Of all the metallurgical variables, grain size appeared to have the greatest effect on fracture morphology particularly at lower stress intensity ranges. While γ' size and distribution are known to affect the fracture mode in fatigue,[11-12] no definite relationship was evident in the present study. This result is not surprising since the purpose of the present investigation was a comparison of seven commercially heat treated turbine disk alloys, while earlier studies on René 95" and Astroloy[12] varied γ' size and distribution in a controlled fashion. Presently, research is underway at NASA to investigate the combined effects of grain size and γ' morphology on crack propagation in low carbon Astroloy at temperatures of interest for turbine disk applications.

Creep-fatigue. - Under creep-fatigue conditions, the fracture morphology of all alloys was predominantly intergranular, as seen in figures 12 to 16. MERL 76 also exhibited fracture sites associated with prior particle boundaries (fig. 15) while Waspaloy was found to crack along twin boundaries on occasion (fig. 16). In both cases fracture was predominantly intergranular as previously stated. Intergranular secondary cracking was present in all alloys and very little cleavage or slip band cracking was observed. Further, there was little change in fracture morphology at higher values of the stress intensity range. Fracture remained predominantly intergranular. The gross ridges shown earlier in figure 5 become more severe as the crack grows. A more detailed view of these ridges (fig. 17) reveals an erratic fracture path with many deep secondary cracks. This behavior differs sharply from the fatigue tests in which the fracture surface is relatively flat and secondary cracks are shallow. While the ridges on the creep-fatigue specimens were associated with cracking along grain boundaries, spacing between adjacent ridges was much larger than the grain size and could not be linked with any other structural feature.

Examination of sections cut perpendicular to the fracture surface did not reveal grain boundary cavities at magnifications up to 3000X. In several instances, oxidized subsurface cracks were observed, as seen in figure 16. However, a majority of the cracks were linked with and appear to have originated at the primary fracture surface. These observations suggest an environmental interaction has accelerated crack growth along grain boundaries.

Under creep-fatigue cycling as under fatigue cycling, the crack growth rates of the high strength, fine grain alloys, IN 100 and NASA IIB-7, were higher than the low strength, coarse grain alloys, Waspaloy and HIP Astroloy. The alloys with a necklace structure H+F Astroloy and René 95, exhibit crack growth rates which were greater than the low strength, coarse grain materials. However, H+F Astroloy was more resistant to crack growth than the high strength, fine grain alloys, while René 95 possessed the highest crack growth rate of all the alloys. Taking necklace grain size as the important parameter in creep-fatigue, the ranking between crack growth rate and grain size holds for H+F Astroloy but does not hold for René 95. The same can be said of the ranking between crack growth rate and strength. In either case, René 95 does not follow the general trend. The presence of PPB fracture sites seems to have affected the crack growth rate of MERL 76 in that stable crack growth conditions could not be produced above 25 MPa $\sqrt{m}$.

Extrapolation of the data does suggest an intermediate crack growth rate which is consistent with the ranking of crack growth rate with strength and grain size.

In summary, creep-fatigue crack growth occurred by an intergranular fracture mechanism regardless of grain size. However, crack growth rates were, in general, lowest for the low strength, coarse grain alloys.

CONCLUSIONS

Fatigue crack propagation at 650° C for seven nickel-base alloys was found to be dependent on cycle type, stress intensity, and microstructure as follows:

(1) Under fatigue loading, the low strength, coarse grain alloys were more resistant to crack propagation than the high strength, fine grain alloys.

(2) Fracture morphology in fatigue was transgranular for alloys with a grain size greater than about 20 μm and intergranular for alloys with a finer grain size. For materials with a necklace structure, fracture was intergranular in the fine, recrystallized grains and transgranular in the coarse grains.

(3) Under creep-fatigue loading, the crack growth rates of all alloys increased substantially. As in fatigue, the low strength, coarse grain alloys were more resistant to crack propagation than the high strength, fine grain alloys. Fracture was predominantly intergranular in all instances.

(4) The behavior of MERL 76 is basically similar to the other coarse grain alloys, but contamination of the larger powder particles produced an additional failure mechanism along the boundaries of these particles. The presence of the prior particle boundaries (PPB's) is thought to have adversely affected the crack growth rates especially at elevated stress levels.

REFERENCES

1. Runkle, J. C.; and Pelloux, R. M.: Micromechanisms of Low-Cycle Fatigue in Nickel-Based Superalloys at Elevated Temperatures. Fatigue Mechanisms, J. T. Fong, ed., ASTM STP-675, American Society for Testing and Materials, 1979, pp. 501-527.
2. Sadananda, K.; and Shahinian, P.: Crack Growth Under Creep and Fatigue Conditions. Creep-Fatigue-Environment Interactions, TMS-AIME Conference Proceedings, Fall Meeting, R. M. Pelloux and N. S. Stoloff, eds., American Institute of Mining, Metallurgical and Petroleum Engineers, 1979, pp. 86-111.
3. Shahani, V.; Popp, H.G.: Evaluation of Cyclic Behavior of Aircraft Turbine Disk Alloys. (General Electric Co.; NASA Contract NAS3-20368.) NASA CR-159433, 1978.
4. Cowles, B. A.; Sims, D. L.; and Warren, J. R.: Evaluation of the Cyclic Behavior of Aircraft Turbine Disk Alloys. (PWA-FR-10299, Pratt & Whitney Aircraft Group; NASA Contract NAS3-20367.) NASA CR-159409, 1978.
5. Cowles, B. A.; Warren, J. R.; and Haake, F. K.: Evaluation of the Cyclic Behavior of Aircraft Turbine Disk Alloys, Pt. 2. (PWA-FR-13153, PTZ, Pratt & Whitney Aircraft Group; NASA Contract NAS3-21379.) NASA CR-165123, 1980.
6. Cowles, B. A.; et al.: Cyclic Behavior of Turbine Disk Alloys at 650° C. J. Eng. Mater. Technol., vol. 102, Oct. 1980, pp. 356-363.

7. Donachie, M. J., Jr.; and Kriege, O. H.: Phase Extraction and Analysis in Superalloys - Summary of Investigations by ASTM Committee E-4 Task Group 1. J. Mater., vol. 7, no. 3, Sep. 1972, pp. 269-278.
8. Annis, C. G., Jr.; Wallace, R. M.; and Sims, D. L.: An Interpolative Model for Elevated Temperature Fatigue Crack Propagation. FR-8042, Pratt & Whitney Aircraft Group, 1976. (AFML-TR-76-176, AD-A038070.)
9. Boyer, Howard E., ed.: Metals Handbook, Vol. 9, Fractography and Atlas of Fractographs. American Society for Metals, 1974, pp. 66-68.
10. Evans, D. J.: MATE: Quarterly Progress Narative Report Project 2, Contract NAS3-20072, September through November 1979, pp. 8-22.
11. Bartos, J. L.: Effect of Microstructure on the Fatigue Crack Growth of a Powder Metallurgy Nickel-Base Superalloy. Ph.D Thesis, Cincinnati, Univ., 1976, pp. 42-78.
12. Laird, C.: The Influence of Metallurgical Structure on the Mechanisms of Fatigue Crack Propagation. Fatigue Crack Propagation, ASTM STP-415, American Society for Testing and Materials, 1967, pp. 131-168, Disc. 169-180.

TABLE I. - CHEMICAL COMPOSITION (WT %) AND HEAT TREATMENTS FOR EACH OF THE SEVEN ALLOYS

Element	Alloy						
	HIP Astroloy	Waspaloy	H+F Astroloy	MERL 76	IN 100	René 95	NASA IIB-7
Al	4.0	1.3	4.1	5.1	5.0	3.6	3.4
Ti	3.5	3.6	3.6	4.2	4.5	2.6	.7
Nb				1.4		3.6	
Ta							10.1
Hf				.48			1.0
Cr	15.1	19.3	14.7	12.0	12.0	12.8	8.9
Mo	5.2	4.2	5.0	3.3	3.1	3.6	2.0
W						3.6	7.6
V					.76		.5
C	.023	.040	.024	.023	.090	.080	.12
B	.024	.005	.027	.020	.019	.010	.023
Zr	<.01	.048	.002	.045	.063	.053	.080
Co	17.0	13.6	17.2	18.4	18.4	8.1	9.1
Ni	Bal.	Bal.	Bal.	Bal.	Bal.	Bal.	Bal.
Solution treatment*	1108/3/AC	1024/4/OQ	1108/4/AC	1163/2/OQ	1121/2/OQ	1092/1/SQ	899/16/to 1094/1/OQ
Aging treatment*	871/8/AC 982/4/AC 649/24/AC 760/8/AC	843/4/AC 760/4/AC	871/8/AC 982/4/AC 649/24/AC 760/8/AC	871/0.7/AC 982/0.7/AC 649/24/AC 760/16/AC	871/0.7/AC 649/24/AC 760/4/AC	760/16/AC	760/16/AC

*Key: 1108/3/AC means 1108° C for 3 hours and air cooled; OQ means oil quench, and SQ means molten salt bath quench

TABLE II. - MECHANICAL PROPERTIES AND FATIGUE

CRACK GROWTH AT 650° C

Material	Tensile strength, MPa	Reduction in area, percent	0.2 percent yield strength, MPa	Fatigue crack growth rate at 30 MPa $\sqrt{m}$, mm/cycle
HIP Astroloy	1234	36.6	881	4.6×10^{-4}
Waspaloy	1262	27.0	957	4.0×10^{-4}
H+F Astroloy	1357	29.3	988	6.6×10^{-4}
MERL 76	1365	25.1	1027	9.4×10^{-4}
IN 100	1380	25.0	1110	9.0×10^{-4}
René 95	1490	14.2	1122	14.4×10^{-4}
NASA IIB-7	1527	10.3	1278	11.3×10^{-4}

TABLE III. - GRAIN SIZE AND GAMMA-PRIME

CONTENT OF EACH ALLOY

Material	Grain size, μm		Gamma-prime content, percent
	Primary	Necklace	
HIP Astroloy	50-70	-----	44
Waspaloy	40-150	-----	20
H+F Astroloy	50-100	10-15	42
MERL 76	15-20	-----	60
IN 100	4-6	-----	62
René 95	50-70	10-15	50
NASA IIB-7	4-6	-----	59

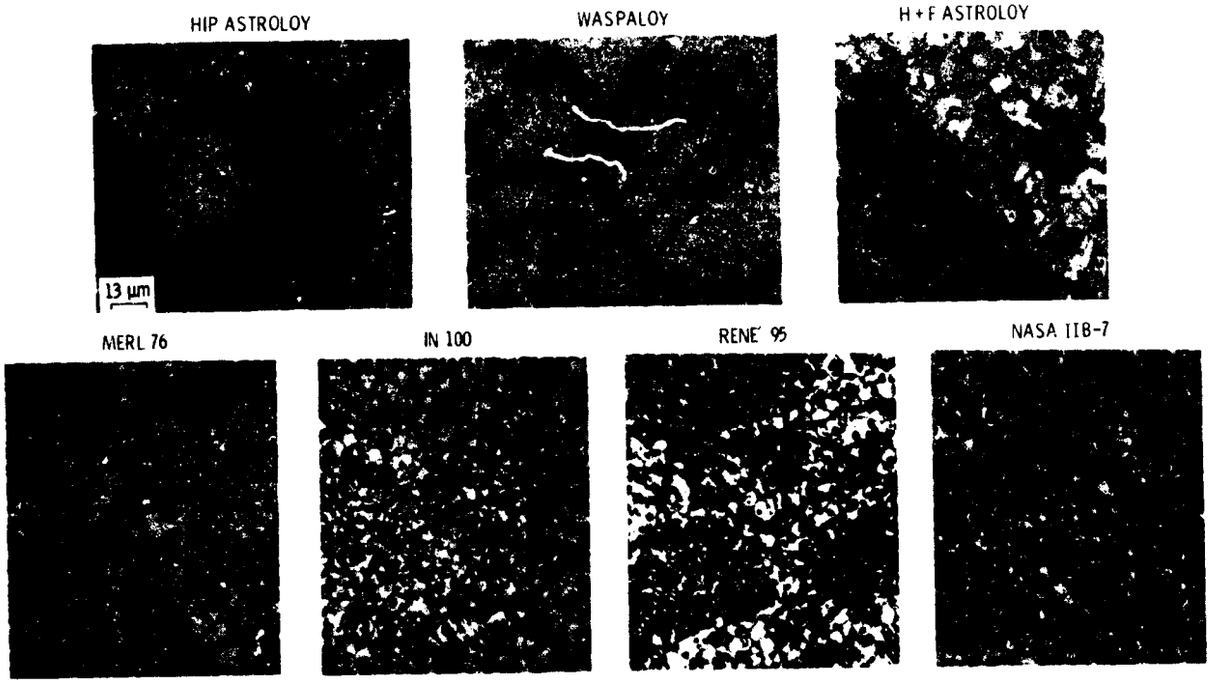

Figure 1. - The microstructures of the seven nickel-base superalloys.

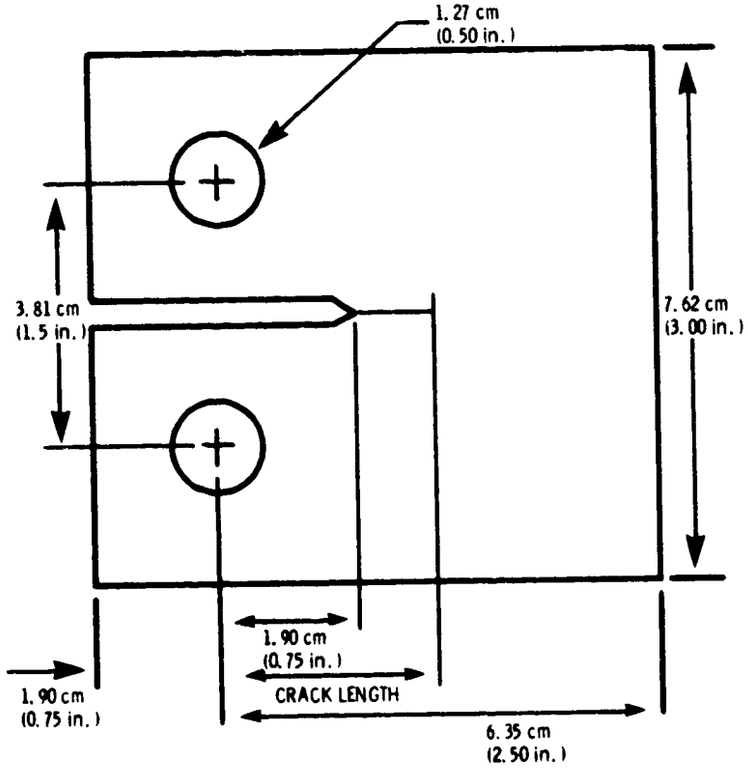

Figure 2. - Design of the compact tension specimen. Thickness of the specimen was 1.25 cm.

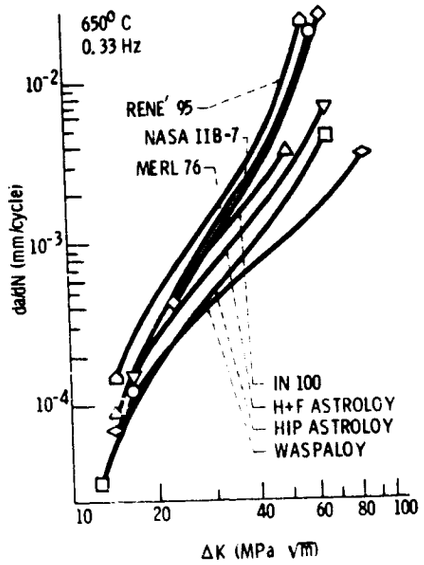

Figure 3. - The crack growth rates of the seven nickel-base superalloys tested in fatigue.[4-6]

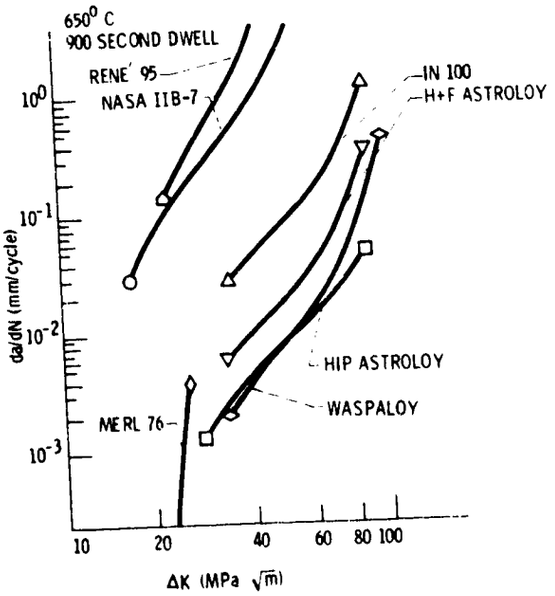

Figure 4. - The crack growth rates of the seven nickel-base superalloys tested in creep-fatigue.[4-6]

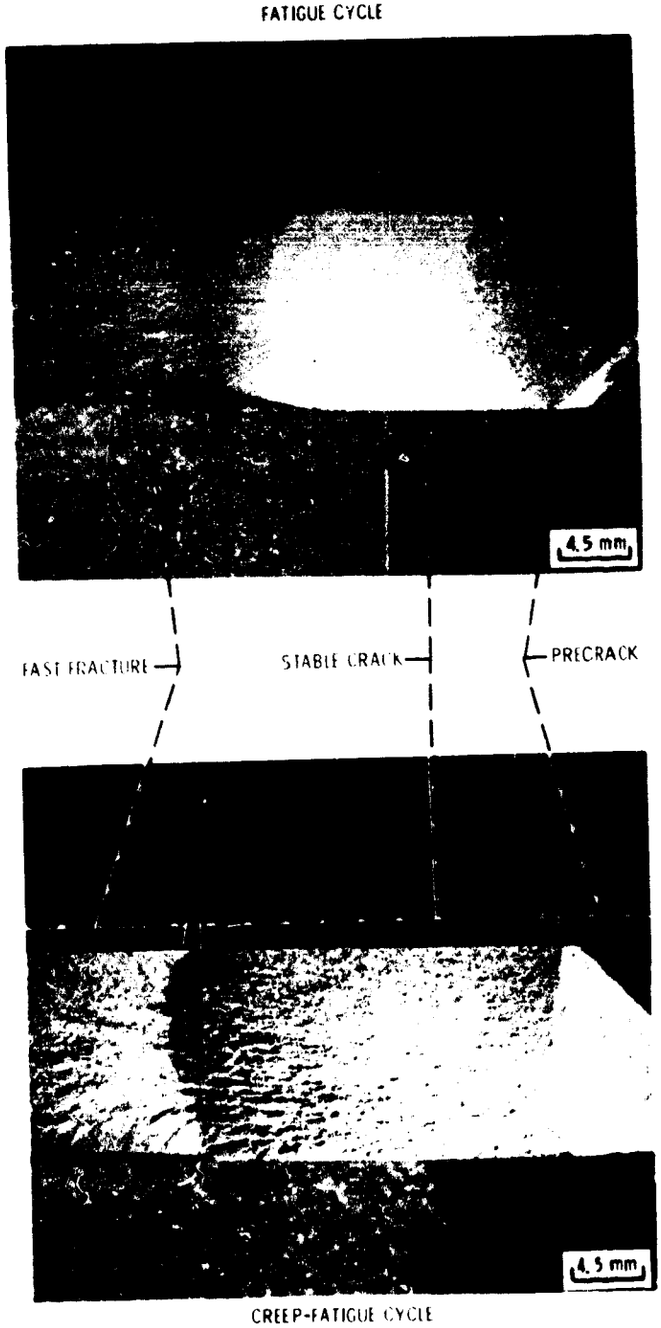

Figure 5. - The fracture surface of the compact tension specimens. Note that in the region of stable crack growth the surface of the fatigue specimen is flat while the creep-fatigue specimen displays ridges which originate at the precrack interface.

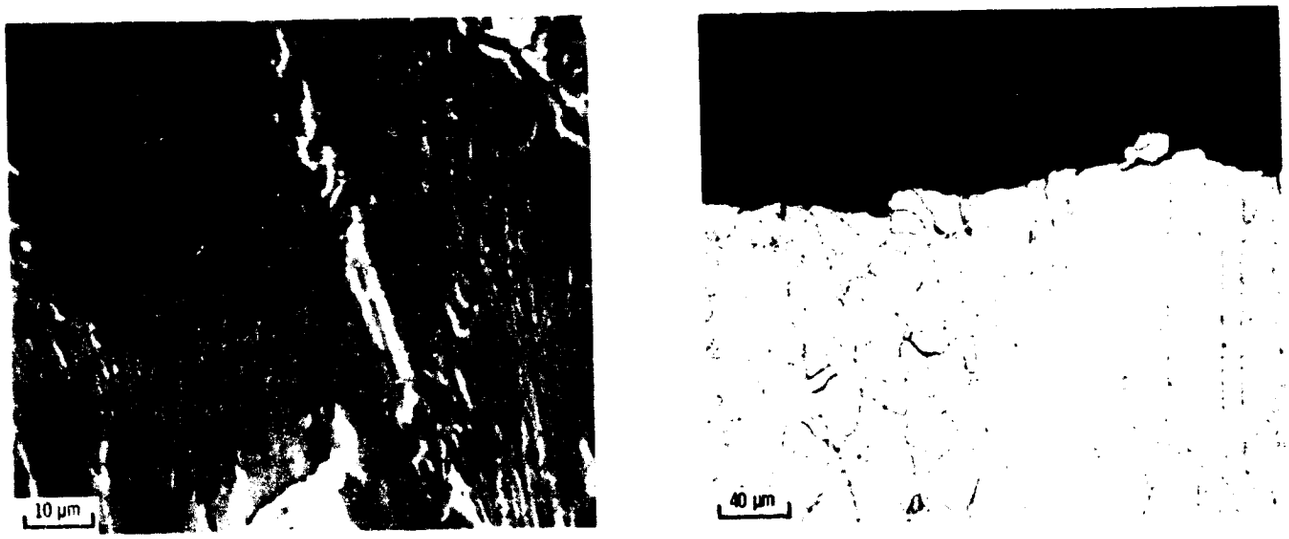

(a) WASPALOY.

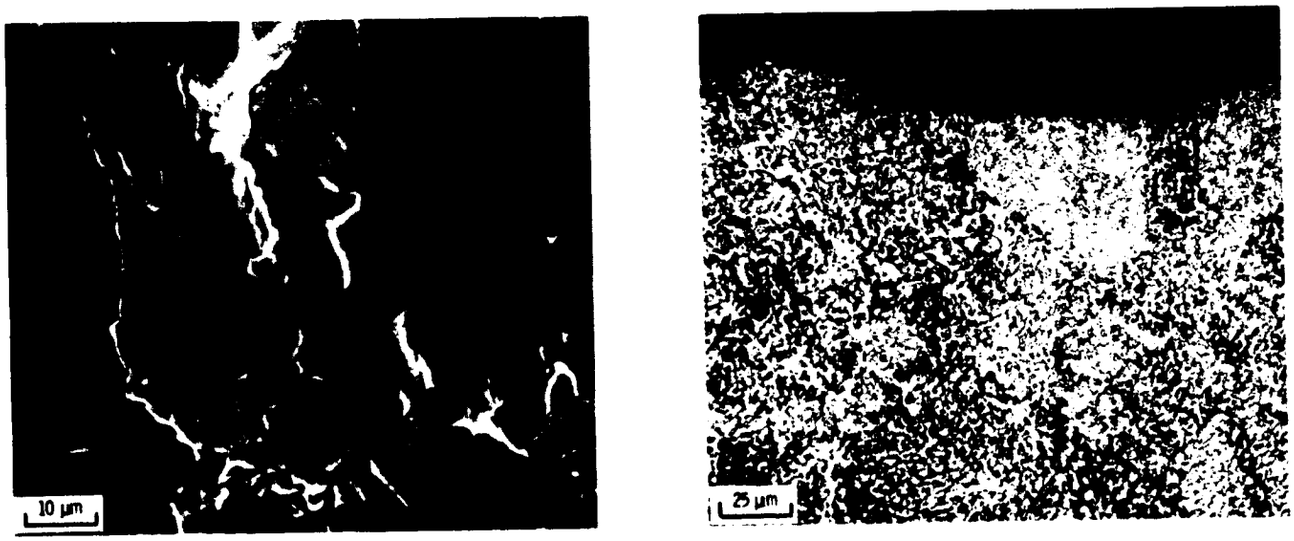

(b) HIP ASTROLOY.

Figure 6 - Transgranular fracture morphology of Waspaloy (a) and HIP Astroloy (b) tested in fatigue. The stress intensity range is approximately 20 MPa $\sqrt{m}$. The direction of crack growth is top to bottom in the sem photos on the left.

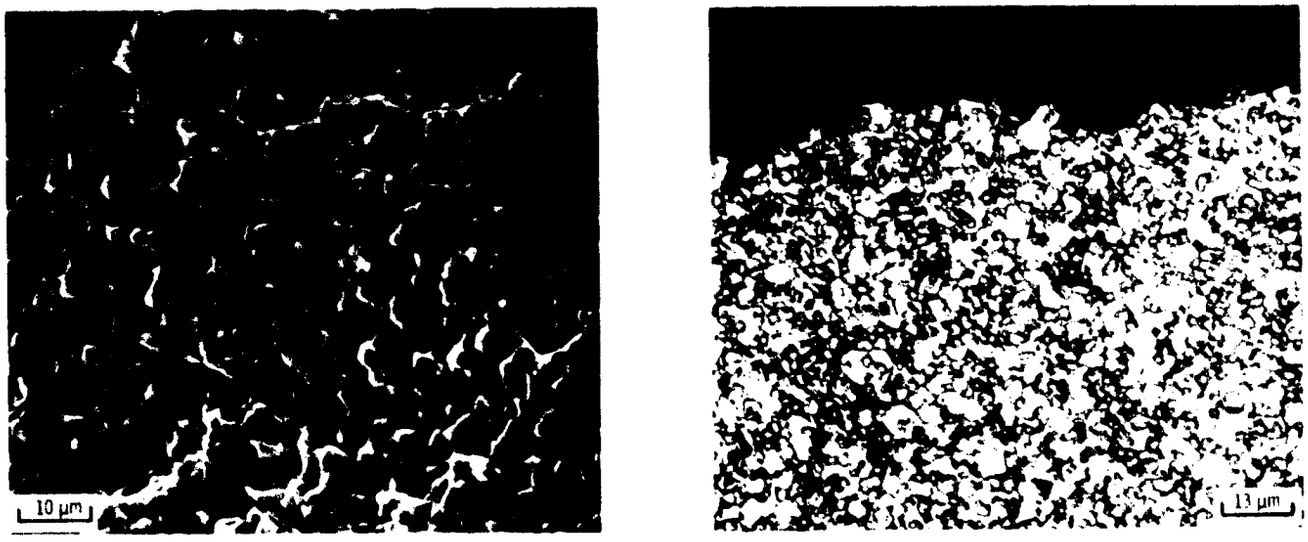

(a) IN 100.

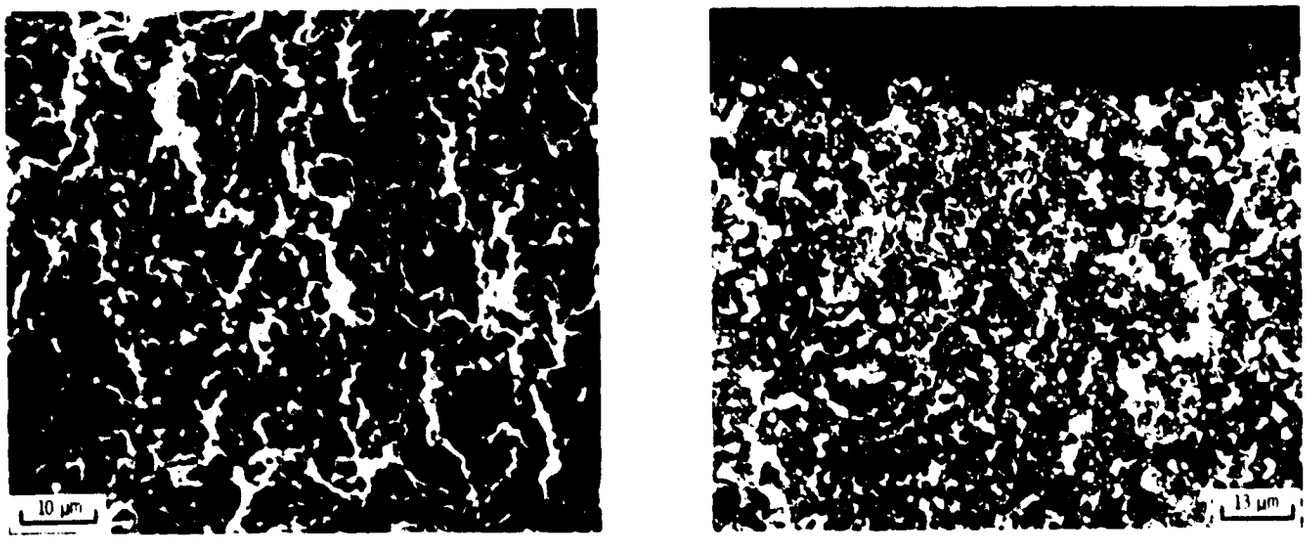

(b) NASA IIB-7.

Figure 7. - Intergranular fracture morphology of IN 100 (a) and NASA IIB-7 (b) tested in fatigue. The stress intensity range is about 20 MPa $\sqrt{m}$. The direction of crack propagation is top to bottom in the sem photos on the left.

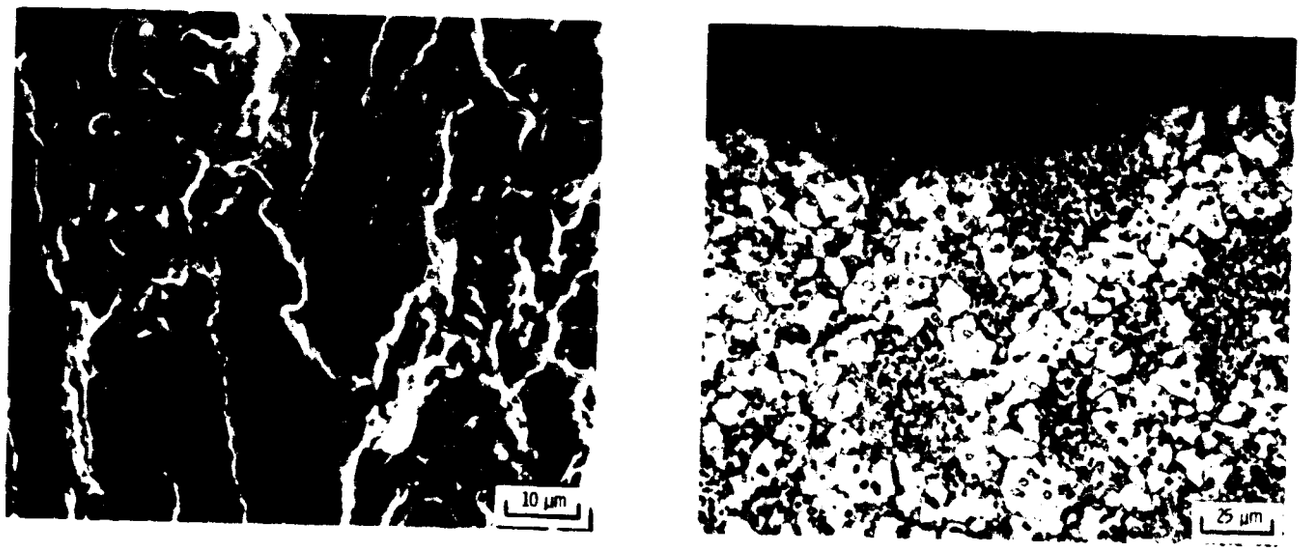

(a) H + F ASTROLOY.

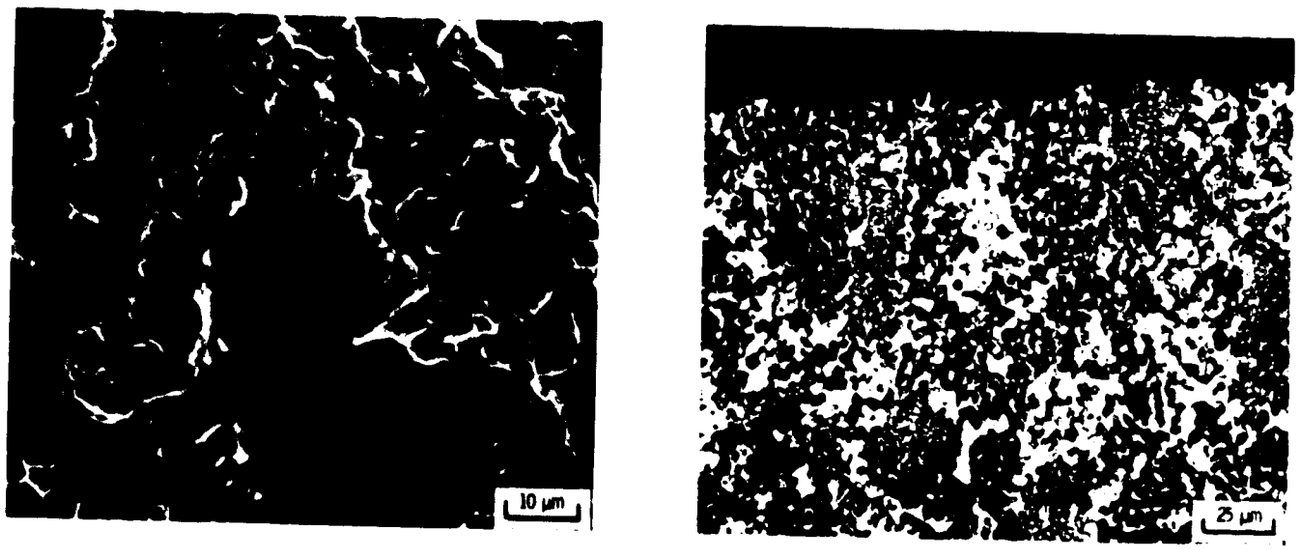

(b) RENE 95.

Figure 8. - Mixed fracture modes in H + F Astroloy (a) and Rene 95 (b) tested in fatigue. The stress intensity range is approximately 20 MPa $\sqrt{m}$. Trans-granular fracture was prevalent in large grains while the fine necklace grains cracked along grain boundaries. Crack growth direction is top to bottom in the sem photos on the left.

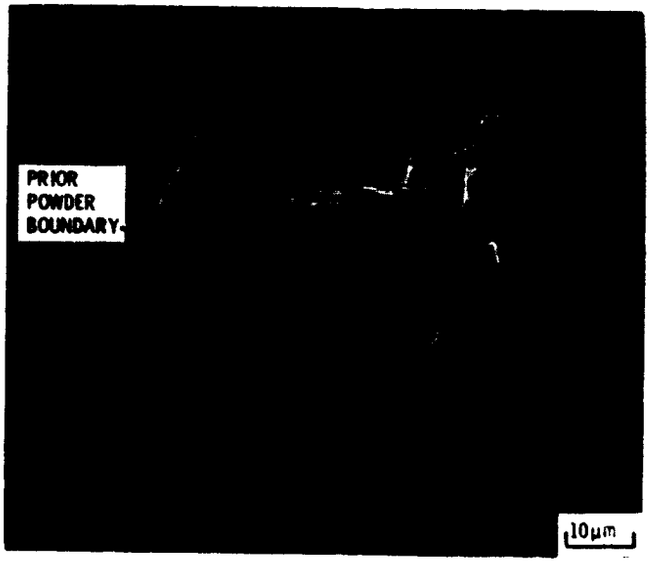

(a)

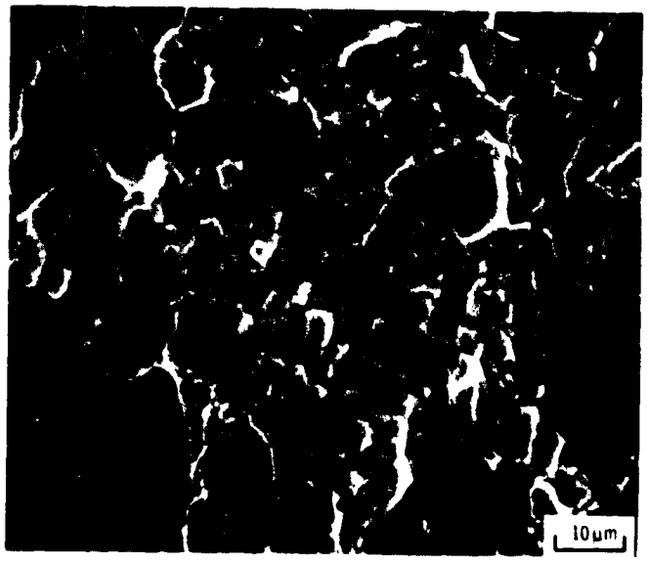

(b)

Figure 9. - A mixed fracture mode at high stresses (a) and transgranular fracture at low stresses (b) were observed in fatigue for MERL 76. The stress intensity range is approximately 30 MPa √m in both photos. The direction of crack growth is top to bottom.

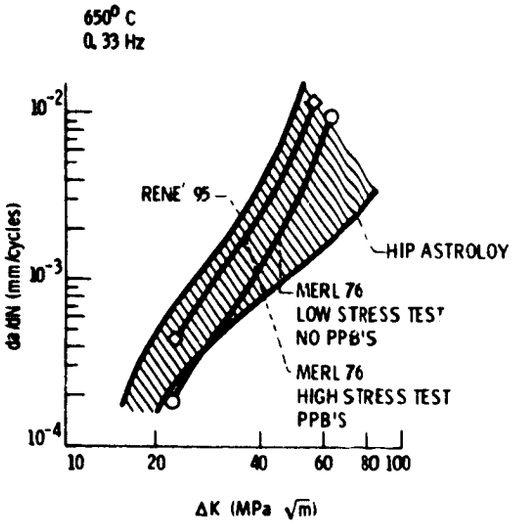

Figure 10. - The effect of prior particle boundaries (PPB) on crack growth rate of MERL 76 tested in fatigue is illustrated above. At lower stress levels, but similar stress intensity ranges, the presence of PPB'S and the crack growth rate for MERL 76 are dramatically reduced, approaching that of HIP Astroloy.

(a) $\Delta K = 20$ MPa $\sqrt{m}$.

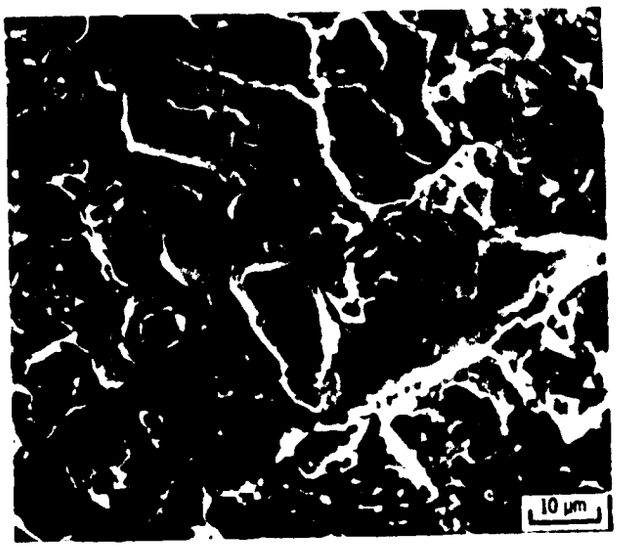

(b) $\Delta K = 45$ MPa $\sqrt{m}$.

Figure 11. - The effect of stress intensity on the fracture morphology of HIP and-forged Astroloy tested in fatigue. Crack growth is influenced by microstructure to a greater degree at lower stress intensities. As the crack grows, secondary cracking is more pronounced and intergranular fracture in the fine grain regions becomes less prominent.

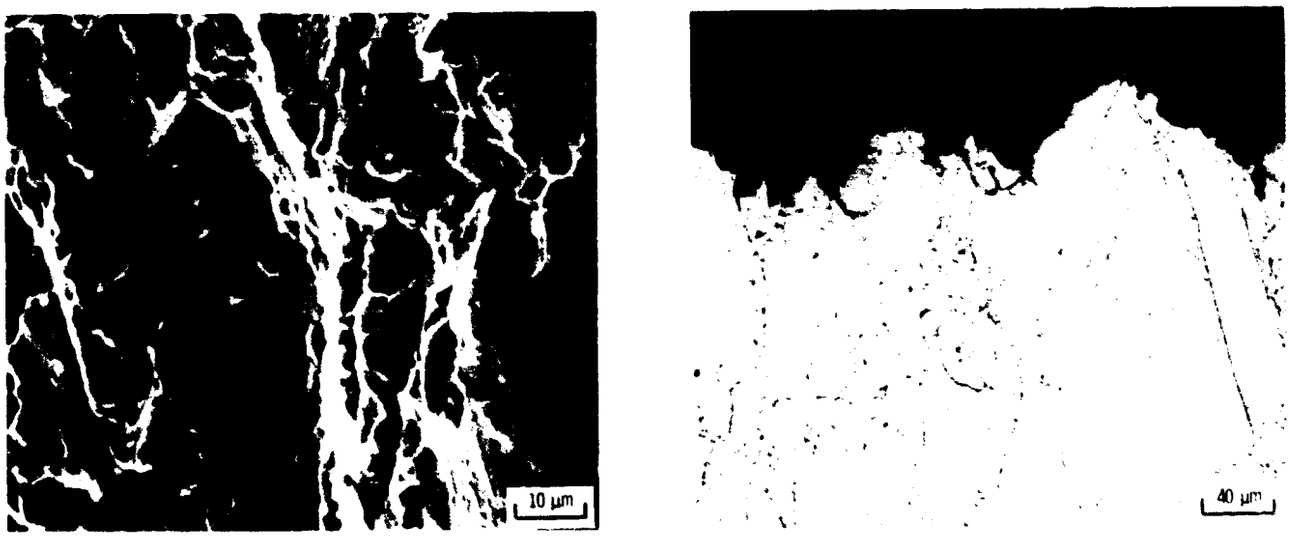

(a) WASPALOY.

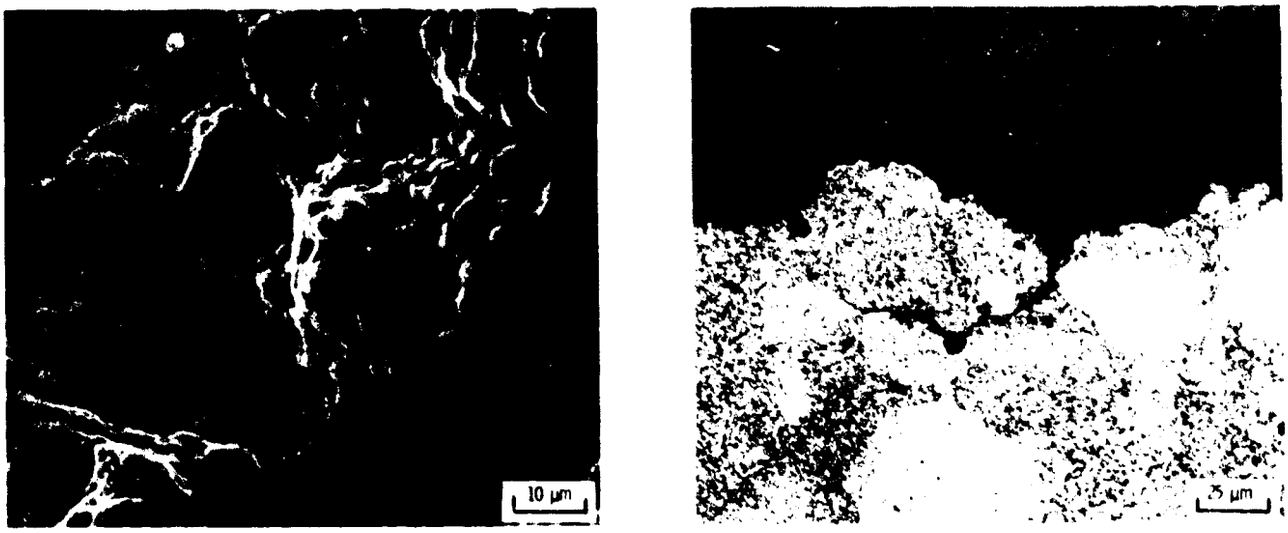

(b) HIP ASTROLOY.

Figure 12. - Intergranular fracture morphology of Waspaloy (a) and HIP Astroloy (b) under creep-fatigue test conditions. The stress intensity range is approximately 35 MPa $\sqrt{m}$. Crack growth direction is top to bottom for the sem photos on the left.

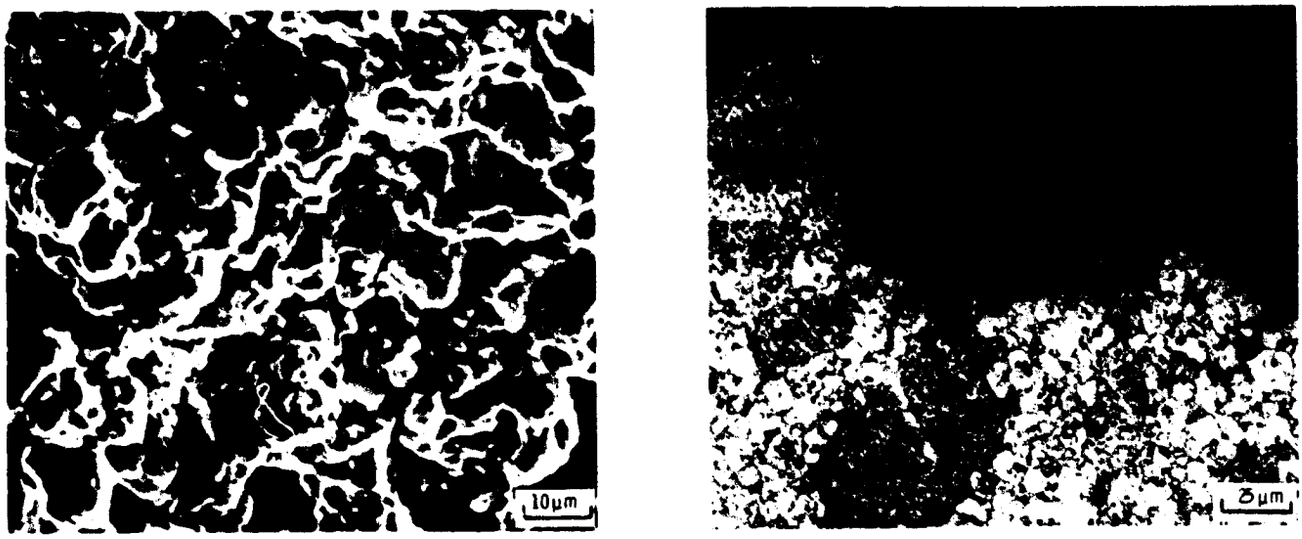

(a) H + F ASTROLOY.

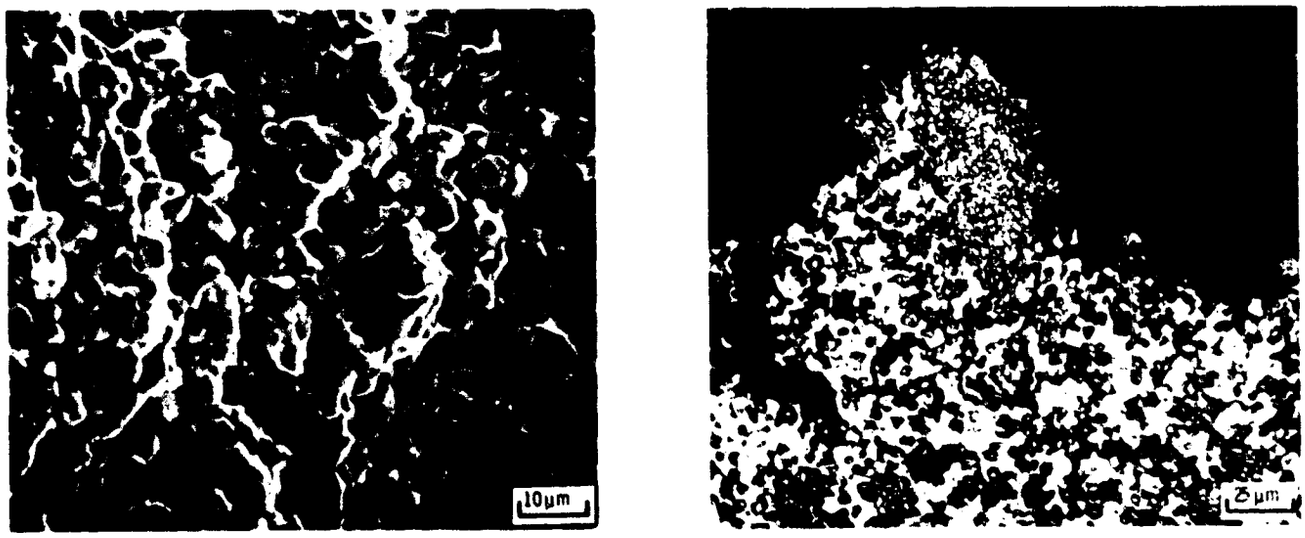

(b) RENE' 95.

Figure 13. - Intergranular fracture morphology of HIP and forged Astroloy (a) and Rene' 95 (b) under creep-fatigue test conditions. The stress intensity range is approximately 35 MPa $\sqrt{m}$ for the Astroloy and 30 MPa $\sqrt{m}$ for the Rene 95. Crack growth direction is top to bottom for the sem photos on the left.

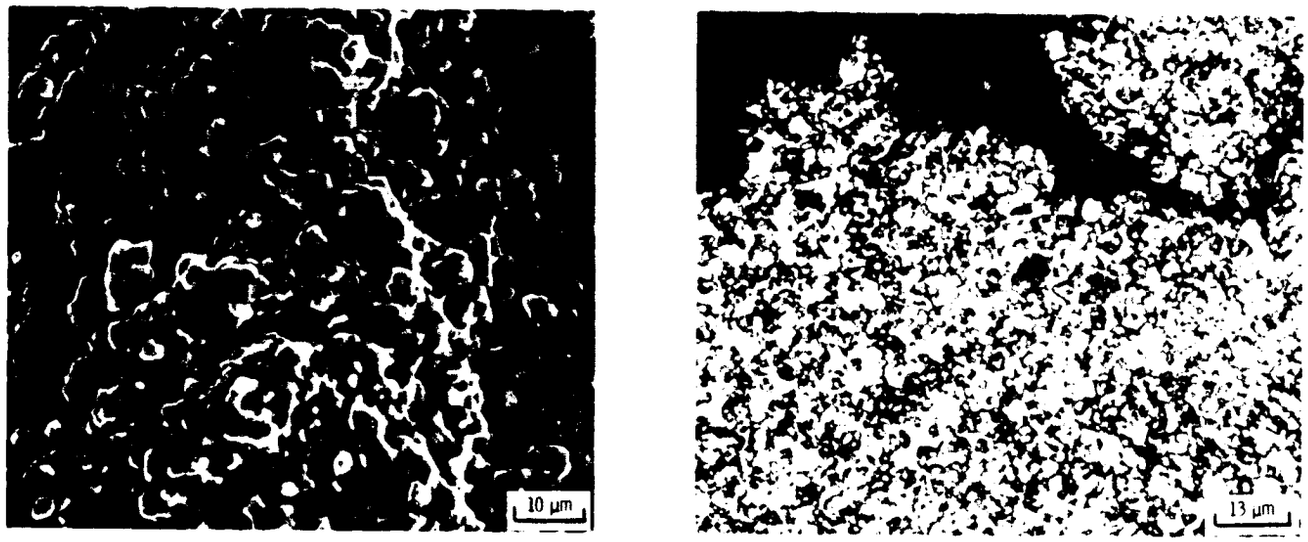

(a) IN 100.

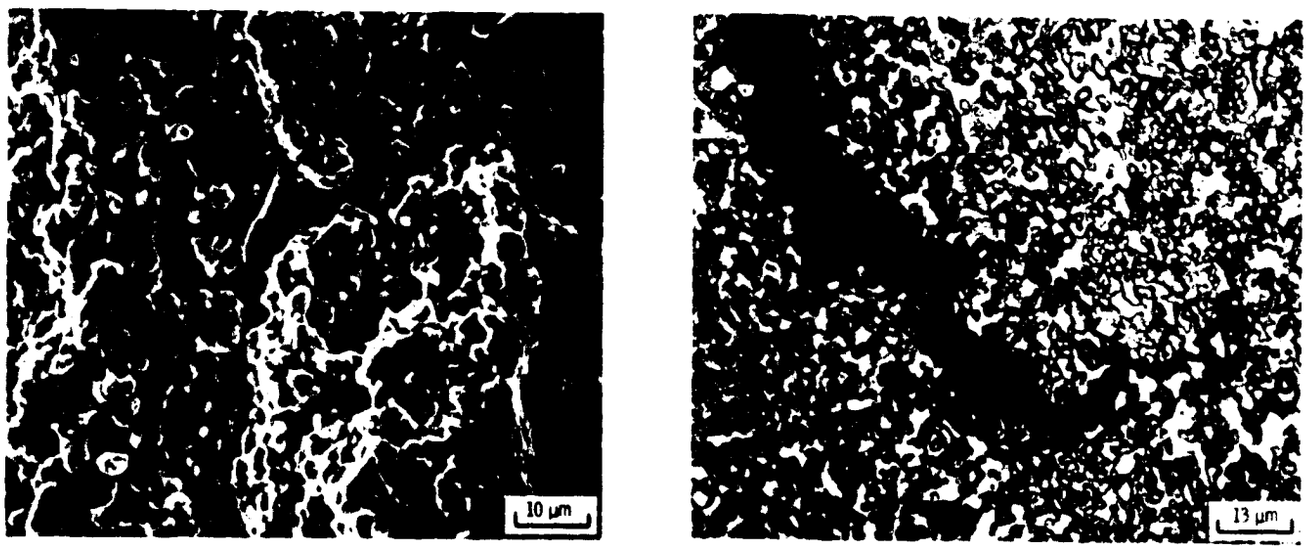

(b) NASA IIB-7.

Figure 14. - Intergranular fracture morphology of IN 100 (a) and NASA IIB-7 (b) under creep-fatigue test conditions. The stress intensity range is approximately 35 MPa $\sqrt{m}$ for IN 100 and 25 MPa $\sqrt{m}$ for NASA IIB-7. Crack growth direction is top to bottom for the sem photos on the left.

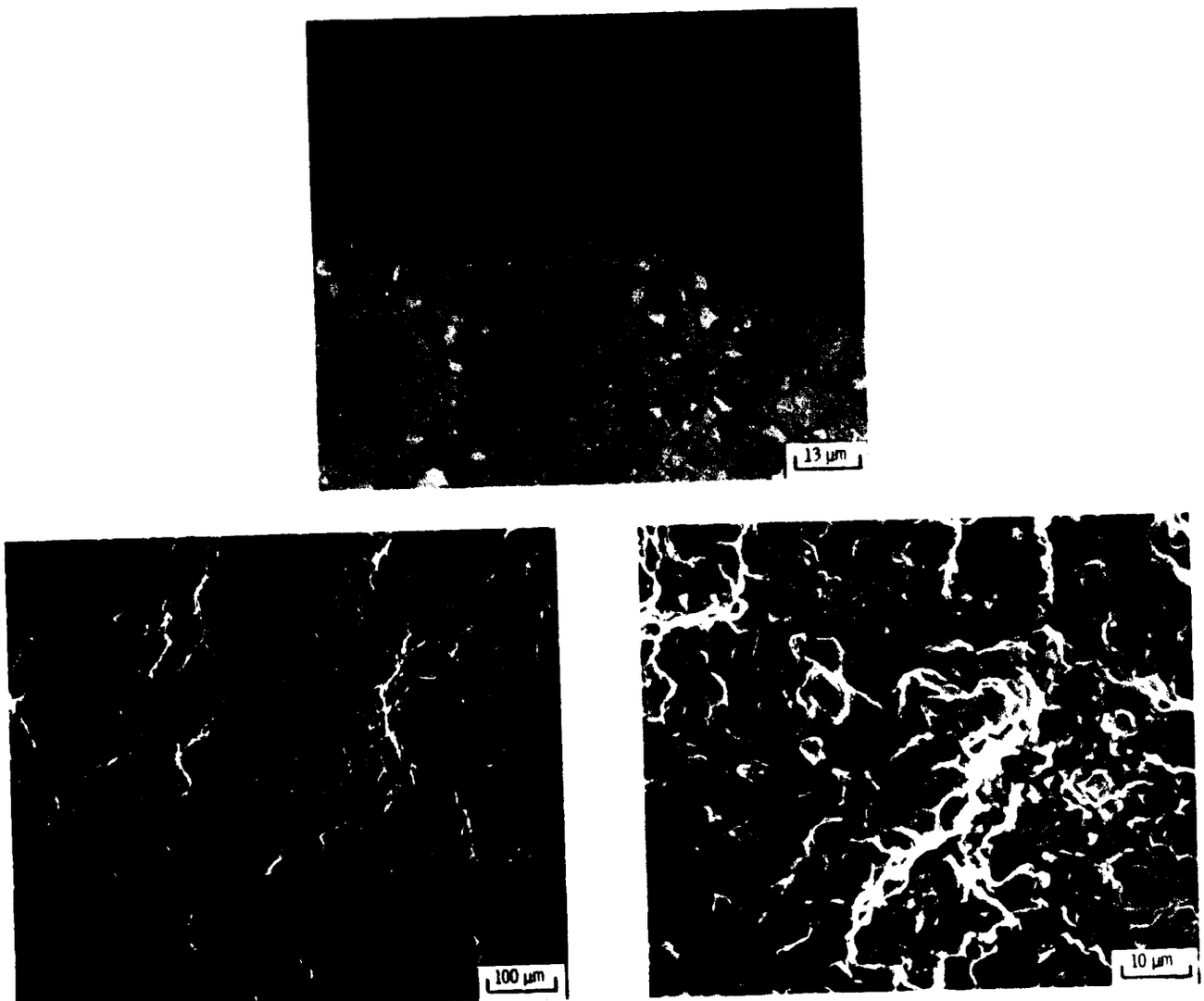

Figure 15. - Mixed fracture mode for MERL 76 under creep-fatigue test conditions. Fracture is predominantly intergranular; however, cracking on prior particle boundaries is observed. The stress intensity range is approximately 3 MPa $\sqrt{m}$. Crack growth direction is top to bottom in the sem photos.

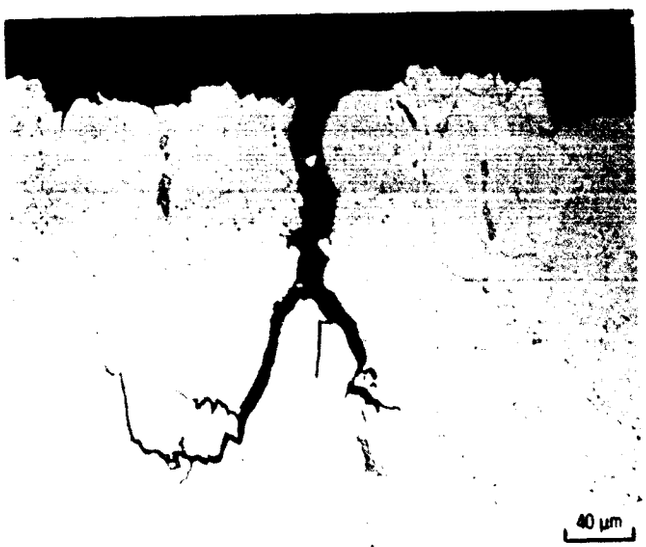

(a) TWIN BOUNDARY CRACKING.

(b) SUBSURFACE CRACKING.

Figure 16 - Secondary cracking in Waspaloy under creep-fatigue test conditions. Fracture occurs along grain boundaries and twin boundaries (a). Subsurface cracks (b) were also observed to a lesser degree.

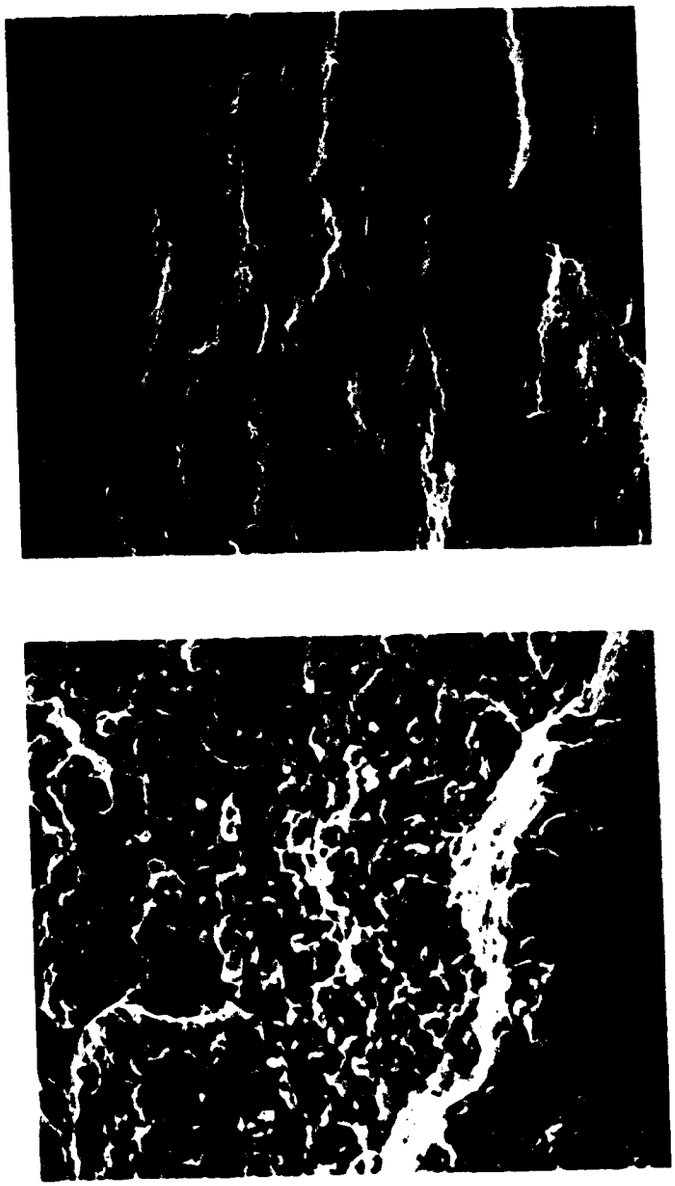

650^{0} C; 900 second dwell

Figure 17. - Detailed view of ridge-like features seen on the creep-fatigue specimens.